

## Modeling and control of a tetrahedron-shaped inverted pendulum with torque-actuation

Tobias Thummerer, Lars Mikelsons

### Angaben zur Veröffentlichung / Publication details:

Thummerer, Tobias, and Lars Mikelsons. 2020. "Modeling and control of a tetrahedron-shaped inverted pendulum with torque-actuation." IFAC-PapersOnLine 53 (2): 17548–55.  
<https://doi.org/10.1016/j.ifacol.2020.12.2667>.

# Modeling and Control of a Tetrahedron-Shaped Inverted Pendulum with Torque-Actuation

Tobias Thummerer\* Lars Mikelsons\*\*

\* Augsburg University, Chair of Mechatronics, 86159 Augsburg, Germany (e-mail: [tobias.thummerer@informatik.uni-augsburg.de](mailto:tobias.thummerer@informatik.uni-augsburg.de))

\*\* Augsburg University, Chair of Mechatronics, 86159 Augsburg, Germany (e-mail: [lars.mikelsons@informatik.uni-augsburg.de](mailto:lars.mikelsons@informatik.uni-augsburg.de))

**Abstract:** This paper provides a methodical procedure for the modeling and control of a tetrahedron-shaped inverted pendulum, balancing on one of its corners. The presented implementation realizes actuation by four motorized reaction wheels with high rotary inertia on the tetrahedron's internal sides. By applying a controlled torque on the tetrahedron's center of mass, the system can be rotated in its environment. The considered system is implemented as a real prototype, which is briefly introduced.

The modeling of the tetrahedron-shaped pendulum leads to a non-linear state space model that can be used for a much greater class of inverted pendulums with arbitrary number of reaction wheels, only by changing the parameterization. Further, the non-linear model is linearized and an appropriate control concept stabilizes the system in one of its instable equilibrium positions: standing on a corner.

Copyright © 2020 The Authors. This is an open access article under the CC BY-NC-ND license (<http://creativecommons.org/licenses/by-nc-nd/4.0>)

**Keywords:** Inverted Pendulum, Tetrahedron, Modeling, Control, Linearization, Reaction Wheel

## 1. INTRODUCTION

In this paper, the tetrahedron-shaped inverted pendulum (henceforth named *TSIP*) is investigated. This pendulum's rigid body housing has a tetrahedron-like shape, but with slightly rounded edges and corners. During the process of balancing, the housing is standing on one of its corners with three rotational degrees of freedom. Throughout this paper, this specific corner is simply identified as *the corner*. To prevent the pendulum from moving too far out of its equilibrium position (and thus from falling), some actuation is required. The inverted pendulum considered here comes with four motor-actuated reaction wheels, from here on called the *actuators*.

Probably the most popular representation of the superordinate class of pendulums and source of inspiration is the *Cubli*-Demonstrator from ETH Zurich, see Gajamohan et al. (2013). This demonstrator's housing has the shape of a cube and stands on one of its corners. The *Cubli*-system is actuated by three reaction wheels with orthogonal rotation axes. In Gajamohan et al. (2012), the demonstrator was extended by a braking system, which allows the cube to switch from a stable into an instable equilibrium without external impact.

Most studies on the topic of torque-actuated inverted pendulums have only focused on the modeling of one specific pendulum. In this contribution, a modeling concept similar to the *Cubli* is generalized to inverted pendulums with an arbitrary number of non-orthogonal reaction wheels and demonstrated using a tetrahedron-shaped system. By providing the resulting non-linear state space representation,

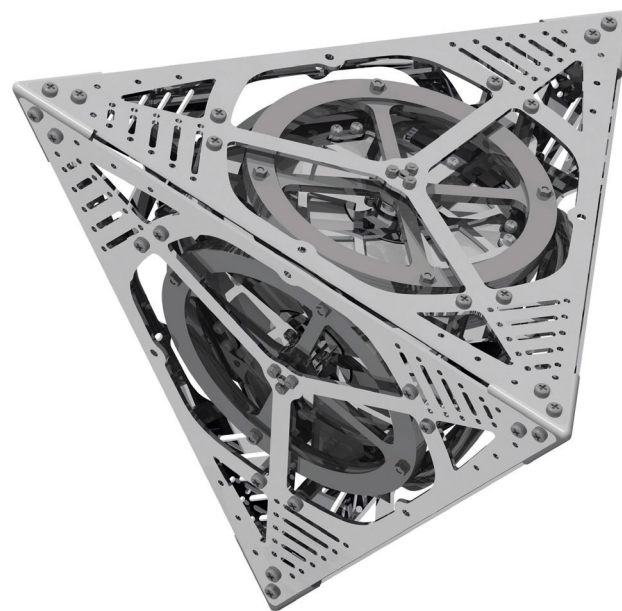


Fig. 1. *TSIP*-Demonstrator without reaction wheel covers.

as well as its linearization, this paper can assist as a quick starting point for the development of similar systems.

Potential applications for a tetrahedron-shaped system are, for example, in education or as oscillation compensator for the mobile platform of a cable robot, similar to Lesellier et al. (2018) and Weber et al. (2014). Another scope of application is the attitude control of spacecrafts as in Weiss et al. (2013), which also uses non-orthogonal reaction wheels.

Even if the discussed procedure focuses on the pendulum balancing on a corner (three degrees of freedom), it can be simplified to the balancing on an edge (one degree of freedom).

This contribution is organized into five technical topics: A short introduction to the *TSIP*-Demonstrator (2), the generalized non-linear state space modeling (3), the model linearization (4), the control design based on the linear model (5) and a short view on the possibilities in case of an over-determined system (6), like the *TSIP* is.

## 2. VIEW ON THE DEMONSTRATOR

Before starting with the modeling and control, this section gives a brief overview on the *TSIP*-Demonstrator, which serves as an implementation example in the upcoming topics. Like the cube, the tetrahedron is a platonic solid. This class of polytopes consists of regular, equal faces (Coxeter, 1973, 4-5), which results in high symmetries and is therefore interesting for modeling and control.

The *TSIP*-Demonstrator<sup>1</sup> (see Fig. 1) consists of a housing out of an aluminum-alloy with four motorized reaction wheels manufactured from high-grade steel. It has an edge length of around  $0.3\text{ m}$  and a total weight of  $3.2\text{ kg}$ . For every face of the tetrahedron, there is one actuator (see Tab. 1) placed at the inside of the housing, precisely behind the face center. The actuators' rotation axes point in direction of the corresponding surface normal.

Table 1. Parameters of the *TSIP*'s actuators.

Parameter	Value	Unit
Weight	0.426	<i>kg</i>
Diameter	0.14	<i>m</i>
Inertia	$1.368 \cdot 10^{-3}$	<i>kg \cdot m^2</i>
Steady torque	0.128	<i>N \cdot m</i>
Steady current	3.21	<i>A</i>
Max. rot. speed	610	<i>rad/s</i>
Rot. damping	$4 \cdot 10^{-5}$	<i>N \cdot m \cdot s/rad</i>

The complete demonstrator consists, in analogy to the four faces, of four almost identical assembly groups. A big advantage of this subdivision is, that as long as all four assembly groups are built up identical and oriented correctly, the CoM (*Center of Mass*) of the resulting tetrahedron-like shape is at its center of geometry, independent of the position of the assembly groups' CoM. Therefore, the CoM of the *TSIP*-Demonstrator is almost<sup>2</sup> at its center of geometry. As in Fig. 2, each assembly group subdivides (from bottom to top) into a reaction wheel cover, the outer housing triangle, the stacked reaction wheel, the inner housing triangle, an electronic mainboard and an electric motor.

Additionally, there are four tetrahedron-shaped corner assembly groups (see Fig. 2, bottom left), that connect the four face assembly groups and serve as mounting platforms for sensors. The demonstrator's translational acceleration vector, angular velocity and heading relative to the earth's magnetic field is measured using four MARG-sensors (*Magnetic, Angular Rate and Gravity*).

<sup>1</sup> Video available: <https://youtu.be/ILqgUaLrwkY>

<sup>2</sup> There is a displacement of about  $0.15 \cdot 10^{-3}\text{ m}$ , because the four face assembly groups are *not* completely identical.

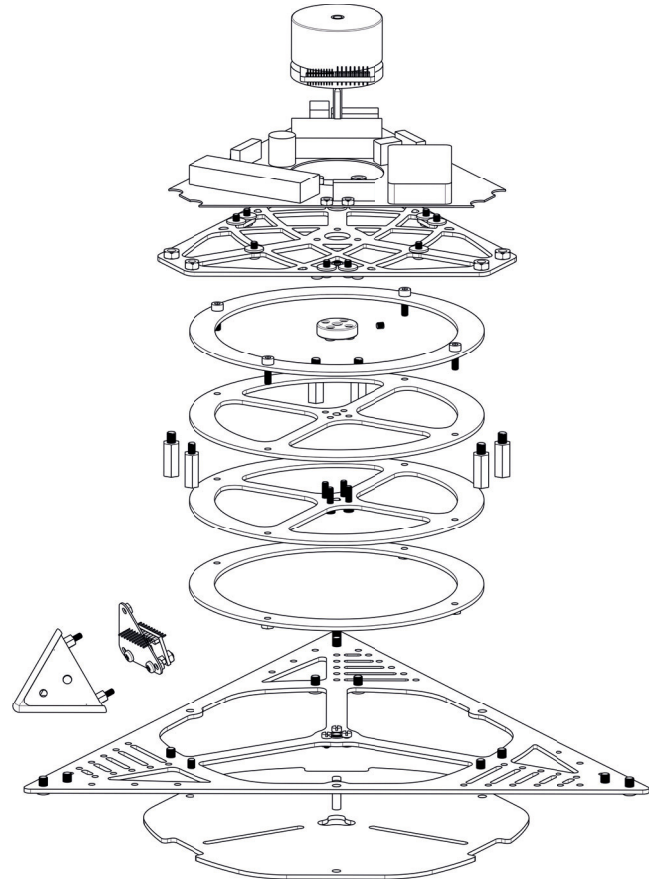


Fig. 2. Face assembly group of the *TSIP*-Demonstrator.

The demonstrator opens up to further extensions, offering installation space and mounting possibilities for additional components, including a mobile power supply or - as in the *Cubli* - a friction break system.

## 3. STATE SPACE MODELING

This section outlines the steps of non-linear modeling, not specialized on a cube- or tetrahedron-shaped system, but a superordinate class of motor-driven three-dimensional inverted pendulums. This class consists of a housing body that is not necessarily a platonic solid, but an arbitrary shape with at least one corner to balance on. There can be any number of actuators, which can be located at different positions and orientations inside the housing and need not be of the same type, meaning they can differ in their mechanical and electrical parameterization. According to the number of actuators, the system's inverse dynamics can be under-determined ( $\leq 2$ ), well-defined ( $= 3$ ) or over-determined ( $\geq 4$ ).

All used coordinate frames are right-handed and orthonormal. A first coordinate frame is positioned at the contact point of the pendulum's corner and the earth's surface with z-axis  $e_{z_I}$  in direction of negative gravity. The x-axis  $e_{x_I}$  and y-axis  $e_{y_I}$  can be selected freely but according to the coordinate system definition. This first frame is simplified as inertial system and therefore it is referenced as the *inertial frame*.

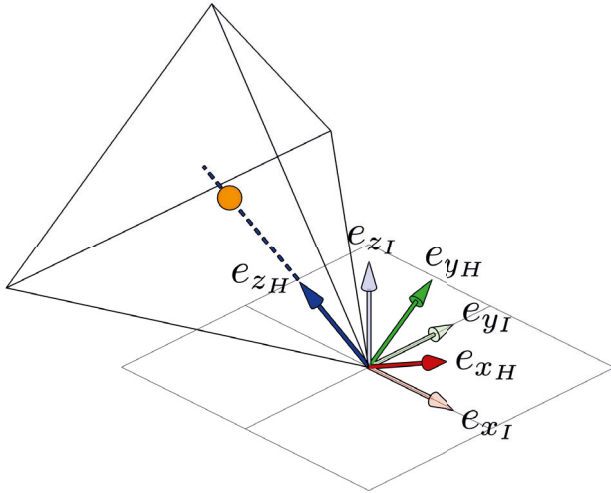


Fig. 3. Inertial and housing coordinate frames.

As in Fig. 3, the second coordinate frame is positioned at the same origin as the inertial frame. The  $z$ -axis  $e_{z_H}$  is defined to point always in direction of the pendulum's CoM (orange). The  $x$ -axis  $e_{x_H}$  points in the heading direction of the housing and the  $y$ -axis  $e_{y_H}$  is completed according to the coordinate system definition. This frame is defined to keep a fixed orientation relative to the housing, therefore it shall not be simplified as inertial system and is further referenced as the *housing frame*. As a consequence, if both coordinate frames are congruent, the multi-body system is exactly in its balance position (no gravitational momentum).

Unless otherwise stated, all variables and parameters are denoted in the housing frame, because of simplifications at the later model parameterization.

### 3.1 State Space Vector

The rigid body system consists of a rigid body housing that is actuated by  $n$  electric motors, each connected with a rigid body reaction wheel that is installed completely inside the housing. Accordingly, the rigid body system counts  $n + 1$  bodies. The corner is modeled connected to the plane ground via a spherical joint. The housing has three rotational degrees of freedom and no translational movement is assumed, for this reason no friction model is deployed.

Each actuator  $i \in \{1, \dots, n\}$  is translational fixed against the housing and has exactly one rotational degree of freedom around its motor axis  $\mathbf{n}_i \in \mathbb{R}^3$ , respectively its rigid body's most inert principal axis of inertia. For a better handling of systems with any number of actuators, let  $\mathbf{N} \in \mathbb{R}^{3 \times n}$  denote the matrix containing all actuators' rotation axes as columns.

To conclude, the system has  $3 + n$  degrees of freedom and therefore the state vector  $\mathbf{x} \in \mathbb{R}^m$  counts  $m = 6 + 2n$  states. The rotation of the housing in the inertial frame is described by the Tait–Bryan-angles  $\psi$  around the axis  $e_{z_I}$  (yaw),  $\theta$  around the axis  $e'_{y_I}$  (pitch) and  $\phi$  around the axis  $e''_{x_I}$  (roll). In general, despite yaw-pitch-roll other rotation conventions are possible. The chosen rotation order leads to a more intuitive control unit design and

parameter tuning, because only a displacement in the roll and pitch angles cause the pendulum to fall. The yaw angle only describes the pendulum's heading. The angle of the actuator  $i$  (motor angle) around its rotation axis is denoted with  $\alpha_i \in \mathbb{R}$ . Thus the state vector reads as:

$$\mathbf{x} = [\phi \ \theta \ \psi \ \alpha_1 \ \dots \ \alpha_n \ \dot{\phi} \ \dot{\theta} \ \dot{\psi} \ \dot{\alpha}_1 \ \dots \ \dot{\alpha}_n]^T \quad (1)$$

The zero position of all states is chosen so that the system's considered equilibrium position is exactly at  $\mathbf{x}_e = \mathbf{0}$ .

The system shall be formulated in state space representation, with the well known state space differential equation:

$$\dot{\mathbf{x}} = \mathbf{f}(\mathbf{x}, \mathbf{u}) \quad (2)$$

Since all states of the system are assumed to be measurable (like they are in the *TSIP-Demonstrator*), the system output  $\mathbf{y} = \mathbf{x}$  is simply defined as the current system state. The system input vector  $\mathbf{u} \in \mathbb{R}^n$  contains the electrical currents running through each motor.

Note, that in Gajamohan et al. (2013), the yaw-Angle of the *Cubli* was assumed to *not* be measurable. This is because the *Cubli* is using IMUs (*Inertial Measurement Unit*) that are missing - compared to MARGs - a magnetometer for attitude detection. In this application, the yaw angle can be determined directly with these integrated magnetometers. Further, the accuracy of these measurement results can be improved by using a sensor fusion algorithm like in Madgwick (2010).

Because the housing's rotation is denoted in the inertial frame (which is more intuitive and helpful for visualizations), but the other states and parameters are defined in the housing frame, it is convenient to convert the housing's rotation into a quantity corresponding to its fixed frame.

Let  $\boldsymbol{\omega} \in \mathbb{R}^3$  denote the system's (and therefore the housing's) angular velocity, calculated as in (3) using the transformation matrix  $\mathbf{T} \in \mathbb{R}^{3 \times 3}$  (Siciliano and Khatib, 2008, 12).

$$\boldsymbol{\omega} = \mathbf{T} \cdot \begin{bmatrix} \dot{\phi} \\ \dot{\theta} \\ \dot{\psi} \end{bmatrix} = \begin{bmatrix} 1 & 0 & -\sin(\theta) \\ 0 & \cos(\phi) & \cos(\theta) \cdot \sin(\phi) \\ 0 & -\sin(\phi) & \cos(\theta) \cdot \cos(\phi) \end{bmatrix} \cdot \begin{bmatrix} \dot{\phi} \\ \dot{\theta} \\ \dot{\psi} \end{bmatrix} \quad (3)$$

Note that the matrix  $\mathbf{T}$  is singular for the values  $\theta = \pm \frac{\pi}{2}$  in the interval  $\theta \in [-\pi; \pi]$ , but due the system's geometry and operation range<sup>3</sup> no singularities can occur inside the real workspace.

### 3.2 Parameters

All parameters that belong to a specific body are indexed with 0 for the housing body and  $i \in \{1, \dots, n\}$  for the actuators' bodies. Every body of the system  $j \in \{0, \dots, n\}$  has a mass  $m_j \in \mathbb{R}^+$  and a position relative to the housing frame  $\mathbf{s}_j \in \mathbb{R}^3$ . For any position vector  $\mathbf{s}_j$ , the corresponding skew symmetric matrix is defined as  $\tilde{\mathbf{S}}_j \in \mathbb{R}^{3 \times 3}$ . The squared skew symmetric matrix  $\tilde{\mathbf{S}}_j^2 \in \mathbb{R}^{3 \times 3}$  shall be defined as  $\tilde{\mathbf{S}}_j \cdot \tilde{\mathbf{S}}_j$ .

<sup>3</sup> Before reaching a critical angle for  $\theta$ , the housing will collide with the plane ground.

Any scalar-matrix-product stands for the element-wise multiplication of the scalar with the matrix' entries.

The inertia tensor of a rigid body is usually defined for rotations about its CoM. The required tensors shall be denoted as  $\mathbf{I}_{0*}$  for the housing and  $\mathbf{I}_{i*}$  for the actuator  $i$ , where the index suffix  $*$  stands for the rotation around the bodies' CoM.

Since the housing does *not* rotate around its CoM, the inertia tensor needs to be transformed via the parallel-axis theorem as follows:

$$\mathbf{I}_0 = \mathbf{I}_{0*} + m_0 \cdot \tilde{\mathbf{S}}_0^T \cdot \tilde{\mathbf{S}}_0 = \mathbf{I}_{0*} - m_0 \cdot \tilde{\mathbf{S}}_0^2 \quad (4)$$

The housing's inertia tensor  $\mathbf{I}_0$  is expected to be determined in the housing frame, meaning no tensor rotation is required.

Each actuator's  $i$  inertia tensor is assumed in the following form:

$$\mathbf{I}_{i*} = \begin{bmatrix} j_i & 0 & 0 \\ 0 & j_i & 0 \\ 0 & 0 & i_i \end{bmatrix} \quad i \in \{1, \dots, n\} \quad (5)$$

where  $i_i \geq j_i$ . The actuator is oriented so that its most inert rotation with inertia  $i_i$  is around the z-axis. The non-diagonal elements are all zero, which means the body is free of any deviation moments. This is a formal limitation but also a major objective at the design process of a reaction wheel.

Inter alia to reduce dependencies between the state differential equations later, the inertia tensors of the actuators are divided into an *active* (+) and *passive* (-) tensor so that:

$$\mathbf{I}_i = \mathbf{I}_{i+} + \mathbf{I}_{i-} \quad i \in \{1, \dots, n\} \quad (6)$$

In addition to the translation of the rotation center, the active and passive inertia tensors of the actuators need to be rotated according to their orientation inside the housing by the rotation matrices  $\mathbf{R}_i \in \mathbb{R}^{3 \times 3}$ :

$$\mathbf{I}_{i+} = \mathbf{R}_i \cdot \begin{bmatrix} 0 & 0 & 0 \\ 0 & 0 & 0 \\ 0 & 0 & i_i \end{bmatrix} \cdot \mathbf{R}_i^T \quad i \in \{1, \dots, n\} \quad (7)$$

$$\mathbf{I}_{i-} = \mathbf{R}_i \cdot \begin{bmatrix} j_i & 0 & 0 \\ 0 & j_i & 0 \\ 0 & 0 & 0 \end{bmatrix} \cdot \mathbf{R}_i^T - m_i \cdot \tilde{\mathbf{S}}_i^2 \quad i \in \{1, \dots, n\} \quad (8)$$

To illustrate, the active part of an actuator's inertia tensor is defined as the subpart, that influences the acceleration of the reaction wheel around its rotation axis. The passive subpart has no effect on the inertia around this rotation axis.

Finally the total system active and passive inertia tensors are defined as:

$$\mathbf{I}_+ = \sum_{i=1}^n (\mathbf{I}_{i+}) \quad (9)$$

$$\mathbf{I}_- = \mathbf{I}_0 + \sum_{i=1}^n (\mathbf{I}_{i-}) \quad (10)$$

Note that the *TSIP* was parameterized from a numerical density approximation based on its manufacturing data set (CAD).

### 3.3 Motor model

The torque generated by each electric motor  $\tau_{mi} \in \mathbb{R}$  around its motor axis is described using the well known DC-motor model:

$$\tau_{mi} = k_i \cdot u_i - d_i \cdot \dot{\alpha}_i \quad i \in \{1, \dots, n\} \quad (11)$$

where the motor constant  $k_i$  denotes the amount of generated torque per ampere current flow. The damping constant  $d_i$  describes the damping torque according to the current angular velocity, is highly dependent on the motor application and must be determined experimentally. Note, that  $u_i$  describes the system input (electrical current through motor).

### 3.4 Balances of Torques

The core idea of the formal modeling is divided up into two intuitive torque balances, both derived from Euler's second law. The first one is focused on one actuator inside the housing's fixed frame: The torque generated by the motor equals the actuator's torque of inertia:

$$i_i \cdot (\ddot{\alpha}_i + \mathbf{n}_i^T \cdot \dot{\boldsymbol{\omega}}) = \tau_{mi} \quad i \in \{1, \dots, n\} \quad (12)$$

The absolute angular acceleration of the actuator subdivides into the acceleration between the motor rotor and stator  $\ddot{\alpha}_i$  and additionally the angular acceleration of the motor stator itself, therefore the housing's acceleration. The expression  $\mathbf{n}_i^T \cdot \dot{\boldsymbol{\omega}}$  simply projects the three-dimensional angular acceleration of the system on the considered rotation axis  $\mathbf{n}_i$  of the actuator.

On the other hand, the three-dimensional angular acceleration  $\dot{\boldsymbol{\omega}}_i \in \mathbb{R}^3$  of the actuator  $i$  can be retrieved by:

$$\dot{\boldsymbol{\omega}}_i = \mathbf{n}_i \cdot \ddot{\alpha}_i \quad i \in \{1, \dots, n\} \quad (13)$$

The original balance of torque from (12) can be extended with (13) into the three-dimensional case and towards an absolute sum over all actuators:

$$\sum_{i=1}^n (\mathbf{I}_{i+} \cdot (\dot{\boldsymbol{\omega}}_i + \dot{\boldsymbol{\omega}})) = \sum_{i=1}^n (\mathbf{n}_i \cdot \tau_{mi}) \quad (14)$$

which can be simplified using (9) to:

$$\mathbf{I}_+ \cdot \dot{\boldsymbol{\omega}} + \sum_{i=1}^n (\mathbf{I}_{i+} \cdot \dot{\boldsymbol{\omega}}_i) = \sum_{i=1}^n (\mathbf{n}_i \cdot \tau_{mi}) \quad (15)$$

The second balance of torque is deployed in the inertial frame, which is characterized by the formalism  $(\dots)_I$ . This balance, as you can see in (16), describes the torque of inertia of the multi-body system  $(\boldsymbol{\tau})_I$  around the spherical joint and the actuators' active torque of inertia  $(\boldsymbol{\tau}_i)_I$  around their corresponding rotation axes. The other side of the equation specifies the only external applied torque: The torque caused by gravity  $(\boldsymbol{\tau}_g)_I$ , which is non-zero if the system is outside its balance position.

$$(\boldsymbol{\tau}_g)_I = (\boldsymbol{\tau})_I + \sum_{i=1}^n (\boldsymbol{\tau}_i)_I \quad (16)$$

with

$$(\boldsymbol{\tau})_I = \mathbf{I} \cdot \dot{\boldsymbol{\omega}} + \boldsymbol{\omega} \times (\mathbf{I} \cdot \boldsymbol{\omega}) \quad (17)$$

and

$$(\boldsymbol{\tau}_i)_I = \mathbf{I}_{i+} \cdot \dot{\boldsymbol{\omega}}_i + \boldsymbol{\omega} \times (\mathbf{I}_{i+} \cdot \boldsymbol{\omega}_i) \quad i \in \{1, \dots, n\} \quad (18)$$

The gravity vector always points in direction of the negative z-axis in the inertial frame. To perform calculations with quantities inside the housing frame, the gravity acceleration vector needs to be rotated along  $\theta$  and  $\phi$  into the housing frame, resulting in the gravity acceleration vector  $\mathbf{z}$ . Note that the gravity vector in the housing frame is independent of the angle  $\psi$ .

$$\mathbf{z} = \begin{bmatrix} \sin(\theta) \\ -\sin(\phi) \cdot \cos(\theta) \\ -\cos(\phi) \cdot \cos(\theta) \end{bmatrix} \cdot g \quad (19)$$

Here,  $g \approx 9.81 \text{ m/s}^2$  denotes the gravitational acceleration.

The force of gravity on a rigid body  $\mathbf{f}_j$  can easily be determined with the help of Newton's second law:

$$\mathbf{f}_j = \mathbf{z} \cdot m_j \quad j \in \{0, \dots, n\} \quad (20)$$

By multiplying the gravitational force with the skew symmetric position matrix of the corresponding body, the torque generated by the gravity force can be calculated. The total generated torque by gravity on the system  $\boldsymbol{\tau}_g$  is simply the sum over all torques:

$$(\boldsymbol{\tau}_g)_I = \boldsymbol{\tau}_g = \sum_{j=0}^n (\tilde{\mathbf{S}}_j \cdot \mathbf{f}_j) = \mathbf{M} \cdot \mathbf{z} \quad (21)$$

For a better reading in the upcoming linearization, the mass distribution of the multi-body system can be stored in the matrix  $\mathbf{M} \in \mathbb{R}^{3 \times 3}$ , which is defined as follows:

$$\mathbf{M} = \sum_{j=0}^n (m_j \cdot \tilde{\mathbf{S}}_j) \quad (22)$$

### 3.5 Non-linear Model

The first balance of torque in (12) can be solved for  $\ddot{\alpha}_i$ :

$$\ddot{\alpha}_i = -\mathbf{n}_i^T \cdot \dot{\boldsymbol{\omega}} + \frac{\tau_{mi}}{i_i} \quad i \in \{1, \dots, n\} \quad (23)$$

Note, that the resulting equation depends on  $\dot{\boldsymbol{\omega}}$  and hence also on the state derivatives  $\dot{\phi}$ ,  $\dot{\theta}$  and  $\dot{\psi}$ .

The second balance of torque according to (16), after substituting (17) and (18) reads:

$$\boldsymbol{\tau}_g = \mathbf{I} \cdot \dot{\boldsymbol{\omega}} + \boldsymbol{\omega} \times (\mathbf{I} \cdot \boldsymbol{\omega}) + \sum_{i=1}^n (\mathbf{I}_{i+} \cdot \dot{\boldsymbol{\omega}}_i + \boldsymbol{\omega} \times (\mathbf{I}_{i+} \cdot \boldsymbol{\omega}_i)) \quad (24)$$

After rearranging this equation to solve for  $\dot{\boldsymbol{\omega}}$ , the resulting differential equation still depends on the variables  $\dot{\boldsymbol{\omega}}_i$  and therefore on the state derivatives  $\ddot{\alpha}_i$ . By further substituting with (15), this dependency can be dissolved:

$$\dot{\boldsymbol{\omega}} = -\mathbf{I}_-^{-1} \cdot (\boldsymbol{\omega} \times (\mathbf{I} \cdot \boldsymbol{\omega}) - \boldsymbol{\tau}_g + \sum_{i=1}^n (\boldsymbol{\omega} \times (\mathbf{I}_{i+} \cdot \boldsymbol{\omega}_i) + \mathbf{n}_i \cdot \tau_{mi})) \quad (25)$$

To summarize, the highest order state derivatives can be written as in (26), whereas  $\boldsymbol{\omega}$  was defined in (3),  $\tau_{mi}$  in (11) and  $\dot{\boldsymbol{\omega}}$  in (25).

$$\begin{bmatrix} \ddot{\phi} \\ \ddot{\theta} \\ \ddot{\psi} \\ \ddot{\alpha}_1 \\ \vdots \\ \ddot{\alpha}_n \end{bmatrix} = \begin{bmatrix} \frac{d}{dt}(\mathbf{T}^{-1}) \cdot \boldsymbol{\omega} + \mathbf{T}^{-1} \cdot \dot{\boldsymbol{\omega}} \\ \frac{\tau_{m1}}{i_1} \\ -\mathbf{N}^T \cdot \dot{\boldsymbol{\omega}} + \vdots \\ \frac{\tau_{mn}}{i_n} \end{bmatrix} \quad (26)$$

As mentioned, this state space differential equation is valid not only for *Cubli* and *TSIP*, but a width range of reaction wheel driven inverted pendulums.

## 4. LINEARIZATION

Because the inverted pendulum is physically limited to operate close to its equilibrium position, the non-linear system from the previous section is linearized and a linear control concept is employed.

The non-linear system is linearized at its operating point with  $\mathbf{x}_e = \mathbf{0}$  and  $\mathbf{u}_e = \mathbf{0}$ . The linearization process results in the matrices  $\mathbf{A} \in \mathbb{R}^{m \times m}$  and  $\mathbf{B} \in \mathbb{R}^{m \times n}$ , whereas the matrices  $\mathbf{C} \in \mathbb{R}^{m \times m} = \mathbf{I}$  and  $\mathbf{D} \in \mathbb{R}^{m \times n} = \mathbf{0}$  need not be considered in the upcoming control unit design. The parameterized representation for the system matrix  $\mathbf{A}$  reads:

$$\mathbf{A} = \left. \frac{\partial \mathbf{f}}{\partial \mathbf{x}} \right|_{x_0, u_0} = \left. \frac{\partial \dot{\mathbf{x}}}{\partial \mathbf{x}} \right|_{x_0, u_0} = \begin{array}{c} \begin{array}{c} \dot{\phi} \\ \dot{\theta} \\ \dot{\psi} \\ \dot{\alpha}_1 \\ \vdots \\ \dot{\alpha}_n \end{array} \begin{bmatrix} \phi & \theta & \psi & \alpha_1 & \dots & \alpha_n & \dot{\phi} & \dot{\theta} & \dot{\psi} & \dot{\alpha}_1 & \dots & \dot{\alpha}_n \\ \mathbf{0}^{3 \times 3} & \mathbf{0}^{3 \times n} & \mathbb{I}^{3 \times 3} & \mathbf{0}^{3 \times n} & & & & & & & & \\ \mathbf{0}^{n \times 3} & \mathbf{0}^{n \times n} & \mathbf{0}^{n \times 3} & \mathbb{I}^{n \times n} & & & & & & & & \\ \mathbf{A}_1 & \mathbf{0}^{3 \times n} & \mathbf{0}^{3 \times 3} & \mathbf{A}_2 & & & & & & & & \\ \mathbf{A}_3 & \mathbf{0}^{n \times n} & \mathbf{0}^{n \times 3} & \mathbf{A}_4 & & & & & & & & \end{bmatrix} \end{array} \quad (27)$$

For a better reading, the matrix  $\mathbf{A}$  was labeled with the state vector  $\mathbf{x}$  (horizontally) and the state vector time derivative  $\dot{\mathbf{x}}$  (vertically).

The matrices  $\mathbf{A}_1 \in \mathbb{R}^{3 \times 3}$ ,  $\mathbf{A}_2 \in \mathbb{R}^{3 \times n}$ ,  $\mathbf{A}_3 \in \mathbb{R}^{n \times 3}$  and  $\mathbf{A}_4 \in \mathbb{R}^{n \times n}$  are defined as follows:

$$\mathbf{A}_1 = \mathbf{I}_-^{-1} \cdot \mathbf{M} \cdot \begin{bmatrix} 0 & g & 0 \\ -g & 0 & 0 \\ 0 & 0 & 0 \end{bmatrix} \quad (28)$$

$$\mathbf{A}_2 = \mathbf{I}_-^{-1} \cdot \mathbf{N} \cdot \text{diag}(d_1, \dots, d_n) \quad (29)$$

$$\mathbf{A}_3 = -\mathbf{N}^T \cdot \mathbf{A}_1 \quad (30)$$

$$\mathbf{A}_4 = -\mathbf{N}^T \cdot \mathbf{A}_2 - \text{diag}\left(\frac{d_1}{i_1}, \dots, \frac{d_n}{i_n}\right) \quad (31)$$

As you can notice, the right column of  $\mathbf{A}_1$  is always zero for the chosen rotation convention.

The parameterized form for the input matrix  $\mathbf{B}$  is defined as:

$$\mathbf{B} = \left. \frac{\partial \mathbf{f}}{\partial \mathbf{u}} \right|_{x_0, u_0} = \left. \frac{\partial \dot{\mathbf{x}}}{\partial \mathbf{u}} \right|_{x_0, u_0} = \begin{array}{c} \dot{\phi} \\ \dot{\theta} \\ \dot{\psi} \\ \dot{\alpha}_1 \\ \vdots \\ \dot{\alpha}_n \\ \ddot{\phi} \\ \ddot{\theta} \\ \ddot{\psi} \\ \ddot{\alpha}_1 \\ \vdots \\ \ddot{\alpha}_n \end{array} \begin{array}{c} u_1 \cdots u_n \\ \mathbf{0}^{3 \times 3} \\ \mathbf{0}^{n \times 3} \\ \mathbf{B}_1 \\ \mathbf{B}_2 \end{array} \quad (32)$$

with the matrices  $\mathbf{B}_1 \in \mathbb{R}^{3 \times n}$  and  $\mathbf{B}_2 \in \mathbb{R}^{n \times n}$ :

$$\mathbf{B}_1 = -\mathbf{I}_-^{-1} \cdot \mathbf{N} \cdot \text{diag}(k_1, \dots, k_n) \quad (33)$$

$$\mathbf{B}_2 = -\mathbf{N}^T \cdot \mathbf{B}_1 + \text{diag}\left(\frac{k_1}{i_1}, \dots, \frac{k_n}{i_n}\right) \quad (34)$$

To conclude, the linearized state space equation can be written as:

$$\dot{\mathbf{x}} = \mathbf{A} \cdot \mathbf{x} + \mathbf{B} \cdot \mathbf{u} \quad (35)$$

Note that, analogous the non-linear system equations, the linearization matrices  $\mathbf{A}$  and  $\mathbf{B}$  are valid for any inverted pendulum of the considered class.

Before going on with the control design, a simple modal order reduction over the state space model is performed: States and their corresponding differential equations that are not relevant for the controller are removed at first. For control, the absolute angles of the motors are irrelevant and thus omitted in the state vector. By removing these entries, the number of states decreases from  $m = 6 + 2n$  to  $m' = 6 + n$ .

From here on, this contribution examines only the at least well-defined ( $n \geq 3$ ) pendulums of the considered class. The observability matrix has full rank  $m'$  and the

reduced, linearized system is therefore fully observable. By investigating the controllability of the system, the result is that the system's controllability matrix does *not* have full rank, but only rank  $m'' = m' - 1$ . Therefore it is *not* fully controllable, which needs to be considered during control design. Of course, this is also the case in the *Cubli*-System.

Thus, Kalman-Transformation according to Kalman (1963) with transformation matrix  $\mathbf{T}_K \in \mathbb{R}^{m' \times m'}$  is used, splitting the system into four algebraically separated parts based on the properties controllability and observability. Because the considered system is fully observable, but has a single non-controllable internal process, the transformed state space vector  $\tilde{\mathbf{x}}$  is separated into only two parts as in (36): the observable-controllable vector  $\tilde{\mathbf{x}}_{oc} \in \mathbb{R}^{m''}$  and a single observable-non-controllable entry  $\tilde{x}_o \in \mathbb{R}$ .

$$\tilde{\mathbf{x}} = \mathbf{T}_K^{-1} \cdot \mathbf{x} = \begin{bmatrix} \tilde{\mathbf{x}}_{oc} \\ \tilde{x}_o \end{bmatrix} \quad (36)$$

The further examination of the observable-non-controllable entry of the transformed state space vector leads to the following structure:

$$\dot{\tilde{x}}_o = \dot{\psi} + \sum_{i=1}^n (c_i \cdot \dot{\alpha}_i) \quad (37)$$

with  $c_i \in \mathbb{R}$ . The factors  $c_i$  are dependent on the actuators' impact on the system's angular momentum along the axis  $e_{z_H}$ . The associated eigenvalue is 0, as a consequence, the uncontrollable state  $\tilde{x}_o$  is constant over time.

A descriptive interpretation of the non-controllable state is that if an actuator's angular velocity is changed by applying torque, the housing's angular velocity around the yaw-axis is affected in the opposite direction (Newton's third law) and the value of  $\tilde{x}_o$  remains unchanged. Therefore, this non-controllable inner process exists not only in the *Cubli*, but also in the *TSIP* and any other pendulum of the considered class.

At the example of the *TSIP*-Demonstrator, the uncontrollable state looks as follows:

$$\tilde{x}_o = \dot{\psi} + 3 \cdot c \cdot \dot{\alpha}_1 - c \cdot \dot{\alpha}_2 - c \cdot \dot{\alpha}_3 - c \cdot \dot{\alpha}_4 \quad (38)$$

with  $c \approx 0.03$ . The actuator 1 (the reaction wheel at the top of the standing tetrahedron) has three times more impact on the rotation around the axis  $e_{z_H}$  than the other actuators, see (42). For an easier point of view, consider only the housing and the actuator 1 involved in the rotation around  $\psi$ . If for example  $\dot{\alpha}_1$  increases by  $\Delta\dot{\alpha}$ , the housing's angular velocity  $\dot{\psi}$  decreases by  $3 \cdot c \cdot \Delta\dot{\alpha}$  and the state  $\tilde{x}_o$  remains unchanged.

As a consequence, the system's equilibrium position can not be reached if the system starts in a state  $\tilde{x}_o \neq 0$ , because there's a conservation of momentum, either in the housing or in one or more of the actuators. However, this is not a problem if the system does start in its equilibrium position, which is the case in the application of the *TSIP*-Demonstrator. Further, a small value for  $\tilde{x}_o$  does not prohibit the pendulum from reaching its balance position with  $\phi = \theta = \psi = 0$  and  $\dot{\phi} = \dot{\theta} = \dot{\psi} = 0$ , but it is not able to drive all reaction wheels' velocities to zero at the same time.

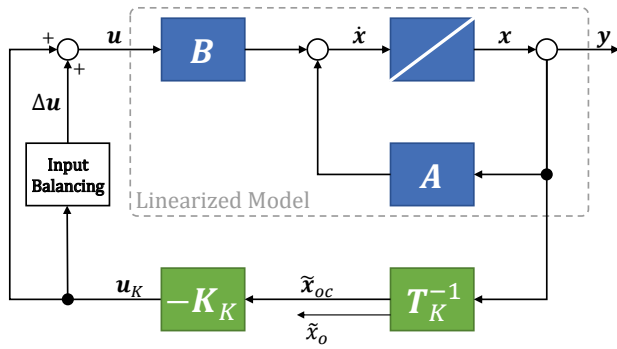


Fig. 4. Closed-loop controlled system.

## 5. CONTROL DESIGN

The open-loop system can be closed by a LQR-based controller. Because the control design should only happen on the controllable part of the system, the system's current state  $\mathbf{x}$  is transformed into the observable-controllable system state  $\tilde{\mathbf{x}}_{oc}$  as in Fig. 4. The non-controllable state vector entry  $\tilde{x}_o$  is simply ignored in the control concept and the later application. The final controlling concept is based on a linear state feedback with gain matrix  $\mathbf{K}_K \in \mathbb{R}^{u \times m''}$ , so that:

$$\mathbf{u}_K = -\mathbf{K}_K \cdot \tilde{\mathbf{x}}_{oc} \quad (39)$$

The feedback gain of an LQ-controller is determined through an optimization problem. The optimization target is to minimize a cost function  $j$  of the following form:

$$\min_{\mathbf{K}_K} j = \int_0^\infty \tilde{\mathbf{x}}_{oc}^T \cdot (\mathbf{Q} + \mathbf{K}_K^T \cdot \mathbf{R} \cdot \mathbf{K}_K) \cdot \tilde{\mathbf{x}}_{oc} dt \quad (40)$$

where  $\mathbf{Q} \in \mathbb{R}^{m'' \times m''}$  and  $\mathbf{R} \in \mathbb{R}^{u \times u}$ .

The elements of the matrices  $\mathbf{Q}$  and  $\mathbf{R}$  are highly dependent on the underlying system parameters and limitations. It is recommended to only fill the diagonal elements of the matrices, because their influence on the optimization can be easier retrieved. The matrix  $\mathbf{R}$  influences the controller in that way, that larger values keep the system input (motor currents)  $\mathbf{u}$  smaller and therefore the settling time (speed of error compensation) decreases. On the other hand, this is helpful to prevent the controller from generating system inputs larger than the physical limitation of the system.

The matrix  $\mathbf{Q}$  assesses the influence of the states on the error compensation. Because the *TSIP*-Demonstrator provides better measurement values for the housing's angular velocity than the housing's absolute angle, the importance of transformed states, that highly depend on these measurement values, was adapted respectively. In addition, the states depending on the angles  $\phi$  and  $\theta$  are weighted more than the states depending on the angle  $\psi$ , because only they cause the pendulum to fall.

## 6. OVER-DETERMINED INVERSE DYNAMICS

An essential difference between the *Cubli* and *TSIP* is, that the inverse dynamics of the *TSIP* is over-determined because of the fourth reaction wheel. As a consequence,

the *TSIP* is able to generate a specific resulting torque on the housing with a variety of system inputs. Compared to the *Cubli*, also the arrangement of the actuators leads to a very different resulting torque. Consider each actuator  $i$  with the rotation axis (respectively the corresponding surface normal)  $\mathbf{n}_i$  deploying the same, non-zero torque  $\tau$ , which leads to a total torque  $\boldsymbol{\tau}_c$  on the *Cubli*:

$$\boldsymbol{\tau}_c = \sum_{i=1}^n \mathbf{n}_i \cdot \tau = \left( \begin{bmatrix} 1 \\ 0 \\ 0 \end{bmatrix} + \begin{bmatrix} 0 \\ 1 \\ 0 \end{bmatrix} + \begin{bmatrix} 0 \\ 0 \\ 1 \end{bmatrix} \right) \cdot \tau = \begin{bmatrix} \tau \\ \tau \\ \tau \end{bmatrix} \quad (41)$$

whereas the total torque  $\boldsymbol{\tau}_t$  on the *TSIP* would be:

$$\boldsymbol{\tau}_t = \left( \begin{bmatrix} 0 \\ 0 \\ 1 \end{bmatrix} + \begin{bmatrix} \sqrt{2}/3 \\ -\sqrt{6}/3 \\ -1/3 \end{bmatrix} + \begin{bmatrix} -\sqrt{8}/3 \\ 0 \\ -1/3 \end{bmatrix} + \begin{bmatrix} \sqrt{2}/3 \\ \sqrt{6}/3 \\ -1/3 \end{bmatrix} \right) \cdot \tau = \begin{bmatrix} 0 \\ 0 \\ 0 \end{bmatrix} \quad (42)$$

Therefore, if all actuators in the *TSIP* are providing the same torque  $\tau$ , the resulting torque on the entire multi-body system is zero. This would also be the case in the *Cubli*, if all six faces of the cubic housing were equipped with an actuator. Furthermore, the relation  $\sum_{i=1}^n \mathbf{n}_i = \mathbf{0}$  is valid for any platonic solid housing with an actuator for every face and rotation axes according to the face normals.

From the view of control, the computed system input is a valid solution to stabilize the pendulum, but it is not unique. Consider that any resulting torque  $\boldsymbol{\tau}_t$  on the tetrahedron can be achieved by linearly combining only the axes' vectors of the reaction wheels 2, 3 and 4. As a consequence, the reaction wheel 1 (on the top of the standing tetrahedron) could be ignored for the balancing process.

According to (42), adding a constant torque  $\Delta\tau$  on all actuator torques does not affect the resulting torque on the linearized multi-body system. This insight allows an intelligent manipulation of the controller output. Although it seems a good idea to modify the controller output dependent on the motor revolution speeds, in practice another more simple approach provides better results: The balancing of the controller output dependent on the maximum  $u_{max} = \max(u_{K1}, \dots, u_{Ki})$  and minimum value  $u_{min} = \min(u_{K1}, \dots, u_{Ki})$  of  $\mathbf{u}_K$  at any time with  $\Delta\mathbf{u}$ :

$$\Delta\mathbf{u} = -\frac{u_{min} + u_{max}}{2} \quad (43)$$

By element-wise adding  $\Delta\mathbf{u}$ , any controller output  $\mathbf{u}_K$  can be transformed to retrieve the balanced system input (see Fig. 4):

$$\mathbf{u} = \mathbf{u}_K + \Delta\mathbf{u} = \mathbf{u}_K + \begin{bmatrix} \Delta u \\ \vdots \\ \Delta u \end{bmatrix} \quad (44)$$

Therefore the controller output can be shifted from the interval  $[u_{min}; u_{max}]$  into the symmetric interval  $[-u_{sym}; u_{sym}]$  with

$$u_{sym} = \frac{u_{max} - u_{min}}{2} \quad (45)$$

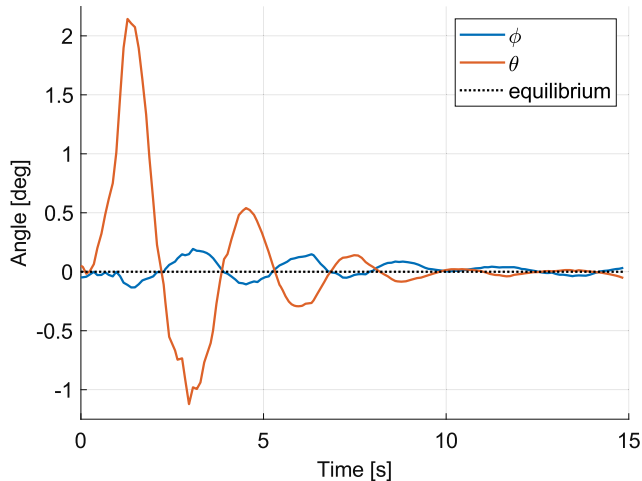


Fig. 5. Housing angles  $\phi$  and  $\theta$ .

As a consequence, motor currents that would exceed the physical limitations, can often be shifted in a realizable interval with equivalent system behavior<sup>4</sup>. Although this adjustment was not necessary to run the system in its equilibrium position, it allows a much better operation performance under heavy or non-vanishing disturbances.

Alternatively, an additional reaction wheel can always be used as an online back-up in case of an actuator malfunction (or deliberately deactivation), simply by picking  $\Delta u$  so, that the inactive actuator's input is zero.

## 7. CONCLUSION & FUTURE WORK

The presented procedure in this paper was used to design an appropriate control unit for the *TSIP*-Demonstrator, which was deployed on an ARM-Microcontroller running with a stable frequency of 200 Hz. The plots show a measurement of the housing's angles  $\phi$  and  $\theta$  (Fig. 5) and the motor currents (Fig. 6) of the real demonstrator, starting the experiment with a manual displacement of  $\theta \approx 2.2^\circ$ . As you can see, the extrema of the system inputs  $\mathbf{u}$  are nearly symmetrical in respect to the time-axis, because of the input balancing post-process.

The tetrahedron-shaped inverted pendulum was shortly defined and exemplified at the *TSIP*-Demonstrator. An approach of non-linear state space modeling for the superordinate class of inverted pendulums was made.

Furthermore, the resulting state space representation was linearized, the non-controllable inner process was examined and a simple LQR-based controller was designed for the considered system class. A possible strategy to deal with the (not necessarily) over-determined inverse dynamics was shortly illustrated.

The *TSIP*-Demonstrator is still an active topic of research and will be extended by multiple features. One upcoming subject is the planning of trajectory movements outside the system's equilibrium position. Furthermore, a non-linear control design could enhance the balancing precision as well as the sensitivity against disturbances.

<sup>4</sup> In case of the linearized system. The non-linear dynamics include the gyroscopic effect caused by the rotating reaction wheels, which is neglected in the linearization because it does not exist for  $\mathbf{u}_0 = \mathbf{0}$ .

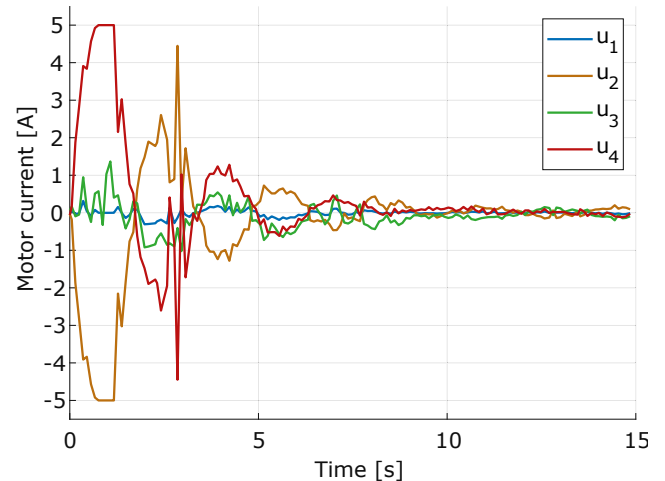


Fig. 6. Motor currents  $\mathbf{u}$  during experiment.

## ACKNOWLEDGEMENTS

The authors like to thank *Pauline Nüsse* for providing suitable components for the cable management inside the demonstrator.

## REFERENCES

- Coxeter, H.S.M. (1973). *Regular Polytopes*. Dover Publications, 3th edition.
- Gajamohan, M., Merz, M., Thommen, I., and D'Andrea, R. (2012). The cubli: A cube that can jump up and balance. *IEEE/RSJ International Conference on Intelligent Robots and Systems (IROS)*, 3722–3727.
- Gajamohan, M., Muehlebach, M., Widmer, T., and D'Andrea, R. (2013). The cubli: A reaction wheel based 3d inverted pendulum. *European Control Conference (Zurich, Switzerland)*, 268–274.
- Kalman, R.E. (1963). Mathematical description of linear dynamical systems. *J.S.I.A.M. Control*, 1(2), 152–192.
- Lesellier, M., Cuvillon, L., Gangloff, J., and Gouttefarde, M. (2018). An active stabilizer for cable-driven parallel robot vibration damping. *IEEE/RSJ International Conference on Intelligent Robots and Systems (IROS)*, 5063–5070.
- Madgwick, S. (2010). An efficient orientation filter for inertial and inertial/magnetic sensor arrays.
- Siciliano, B. and Khatib, O. (2008). *Springer Handbook of robotics*. Springer-Verlag Berlin Heidelberg.
- Weber, X., Cuvillon, L., and Gangloff, J. (2014). Active vibration cancelling of a cable-driven parallel robot using reaction wheels. *IEEE/RSJ International Conference on Intelligent Robots and Systems (IROS)*, 1724–1729.
- Weiss, A., Kolmanovsky, I., Bernstein, D.S., and Sanyal, A. (2013). Inertia-free spacecraft attitude control using reaction wheels. *Journal of Guidance, Control and Dynamics 2013*, 36(5), 1425–1439.